

CALIBRATOR DESIGN FOR THE *COBE*¹ FAR INFRARED ABSOLUTE SPECTROPHOTOMETER (FIRAS)

J. C. MATHER,² D. J. FIXSEN,³ R. A. SHAFER,² C. MOSIER,² AND D. T. WILKINSON⁴

Received 1998 June 5; accepted 1998 September 28

ABSTRACT

The photometric errors of the external calibrator for the Far Infrared Absolute Spectrophotometer (FIRAS) instrument on the *COBE* are smaller than the measurement errors on the cosmic microwave background radiation (CMBR) spectrum (typically 0.02 MJy sr^{-1} , 1σ) and smaller than 0.01% of the peak brightness of the CMB. The calibrator is a reentrant cone, shaped like a trumpet mute, made of Eccosorb iron-loaded epoxy. It fills the entire beam of the instrument and is the source of its accuracy. Its known errors are caused by reflections, temperature gradients, and leakage through the material and around the edge. Estimates and limits are given for all known error sources. Improvements in understanding the temperature measurements of the calibrator allow an improved CMB temperature determination of $2.725 \pm 0.002 \text{ K}$.

Subject headings: cosmic microwave background — cosmology: observations — instrumentation: spectrographs

1. INTRODUCTION

We describe and analyze the performance of the blackbody calibrator for the Far Infrared Absolute Spectrophotometer (FIRAS) instrument on the *Cosmic Background Explorer (COBE)* satellite. The *COBE* (Mather 1982, 1987; Mather et al. 1993; Boggess et al. 1992) was launched on 1989 November 18 on a Delta rocket and carried three instruments to measure the diffuse infrared and microwave background radiation. The primary goal of the FIRAS (Mather et al. 1993) was to compare the cosmic microwave background radiation (CMBR) spectrum to a blackbody spectrum, the predicted ideal result of a hot big bang. Even small deviations from the blackbody form would be important to cosmology, but none have been found.

FIRAS results include limits on the distortion of the CMBR spectrum (Mather et al. 1994; Fixsen et al. 1996), the interpretation of these limits (Wright et al. 1994), measurements of the line emission of the Galaxy (Bennett et al. 1994), a measurement of the CMBR dipole caused by the Sun's motion (Fixsen et al. 1996), and a measurement of the spectrum of the intrinsic anisotropy (Fixsen et al. 1997). The process of calibrating the instrument is described by Fixsen et al. (1994). The data are available from National Space Science Data Center (NSSDC)⁵ and are described extensively in the FIRAS Explanatory Supplement (Brodd et al. 1997). The weighted rms deviation between the CMBR and the calibrator blackbody is only 0.005% of the peak brightness over the frequency range of $2\text{--}20 \text{ cm}^{-1}$ ($5\text{--}0.5 \text{ mm}$ wavelength). The transfer of this result to an absolute statement about the CMBR spectrum depends on the accuracy of the blackbody calibrator, which is the subject of this

paper. The measured deviations are an order of magnitude smaller than the accuracy that was originally required in the instrument design, so it is appropriate to review the main sources of calibrator errors.

The FIRAS spans the frequency range $\nu = 1\text{--}97 \text{ cm}^{-1}$ in two spectral bands divided at 20 cm^{-1} . It has a spectral resolution $\Delta\nu/\nu \sim 0.0035$ (FWHM) limited by beam divergence and an unapodized $\Delta\nu \sim 0.4 \text{ cm}^{-1}$ limited by the maximum path difference of 1.2 cm (0.09 cm^{-1} and 5.6 cm for the long or high-resolution data, respectively). The spectral resolution is obtained with a Fourier transform spectrometer based on the Martin & Puplett (1970) polarizing form of the Michelson interferometer. It is fully symmetrical, with separation of the two input and two output ports (Fig. 1). The inputs are coupled to a reference and the sky or external calibrator. All wavelengths are measured simultaneously with the same detector and the same optical path.

The radiation accepted from the sky comes from a circle 7° in diameter that is defined by a Winston cone (Welford & Winston 1978; Mather 1981; Miller, Eichhorn, & Mather 1982), also designated the sky horn. The sky horn concentrates the beam into a circular aperture $(1.5/\pi)^{1/2} \simeq 0.78 \text{ cm}$ in diameter. The sky horn is a nonimaging device that scrambles the radiation paths. The sky horn and instrument transmit an étendue of $A\Omega = 1.5 \text{ cm}^2 \text{ sr}$. The number of independent geometrical modes of the diffracted radiation field is $n = 2A\Omega\nu^2$, where the factor of 2 allows for polarization states, permitting operation at frequencies as low as 1 cm^{-1} .

Radiation passing through this aperture is focused into the spectrometer by a similar elliptical concentrating cone. Radiation not passing through the aperture is returned to the sky or calibrator, except for a fraction lost by absorption in the cone walls. The absorption of the sky horn was measured in flight by changing the concentrator temperature to determine the emissivity of the combined parabolic and elliptic cones. The horn emissivity is approximately $0.012 + 0.0015 \text{ cm} \times \nu$ in the low-frequency channel ($2\text{--}20 \text{ cm}^{-1}$). By Kirchhoff's law, the emissivity ϵ and the reflectivity r are related by $\epsilon + r = 1$. The calibrator and cone form a cavity in which most of the radiation incident on the surface of the calibrator was originally emitted by the calibrator and has the same temperature. This fact

¹ The National Aeronautics and Space Administration Goddard Space Flight Center (NASA GSFC) was responsible for the design, development, and operation of the Cosmic Background Explorer (*COBE*). GSFC was also responsible for the development of the analysis software and for the production of the mission data sets. The *COBE* program was supported by the Astrophysics Division of NASA's Office of Space Science and Applications.

² NASA Goddard Space Flight Center.

³ Raytheon STX.

⁴ Princeton University.

⁵ <http://www.gsfc.nasa.gov/astro/cobe>.

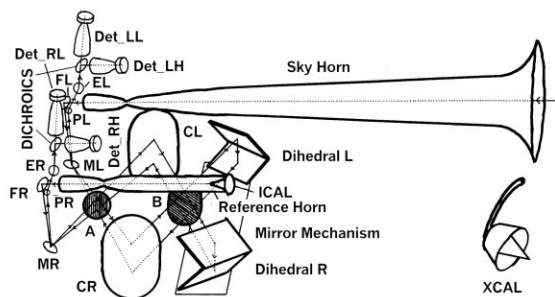


FIG. 1.—Drawing of the FIRAS instrument. Light enters the sky horn from the sky or the XCAL and the reference horn from the ICAL. After reflection from the folding flats (FL, FR), it bounces off the mirrors (ML, MR) and is analyzed by the polarizer (A). The collimator mirrors (CL, CR) recollimate the light before it is split by a second polarizer (B) at 45° . It is then reflected by the dihedral mirrors, with different paths set by the mirror mechanism. After reflection, the light retraverses the beam splitter, collimator mirrors, and analyzer. This time it is intercepted by the pickoff mirrors (PL, PR), which direct it into the elliptical mirrors (EL, ER), the dichroic filters, and, finally, the detectors (Det_LH, Det_LL, Det_RH, Det_RL).

relaxes the requirement on the reflectivity of the calibrator by more than an order of magnitude.

The input end of the Winston cone is connected to a flared section like a trumpet bell, which suppresses diffracted sidelobes over a wide spectral band. Sidelobe measurements have been reported (Mather et al. 1986) and are in good agreement with the calculations based on the geometrical theory of diffraction (Levy & Keller 1959). The smooth transition to a curved flare also suppresses diffraction at the aperture, which would otherwise enable the instrument to see itself through diffracted backscatter.

The entire instrument is operated in a vacuum and cooled to 1.5 K by conduction to a superfluid liquid helium tank. A large external conical shield protects the cryostat and instruments from direct radiation from the Sun and the Earth. The Sun never illuminates the instruments or cryostat, but the *COBE* orbit inclination combined with the inclination of the Earth's equator to the ecliptic do allow the Earth limb to rise a few degrees above the plane of the instrument and sunshade apertures during about one-sixth of the orbit for one-fourth of the year. During this period, the sky horn could not be cooled to 2.7 K because of the Earth limb heating. The edge of the shield is approximately coplanar with the entrance aperture of the FIRAS instrument, so there is no line-of-sight path for radiation from the shield into the instruments. The calibrator and its support arm project above the aperture plane and are exposed to radiation from the warm parts of the cryostat and shade. The effects of this radiation are reduced by multilayer insulation and are estimated below. The temperatures reached during the illumination by the Earth limb are described by Mosier (1991).

The other input (the reference input) also had a Winston cone, although a smaller one, and a calibrator (the internal calibrator or ICAL [Fig. 2]). To match the emission properties, the length-to-diameter ratio for this reference cone (reference horn) was similar to that of the main input cone (sky horn). The ICAL was mounted in the reference horn and could not be moved. It is similar in some respects to the main calibrator (XCAL). The ICAL and reference horn were useful in that they provided a signal much like that of the sky and the sky horn. Because the interferometer mea-

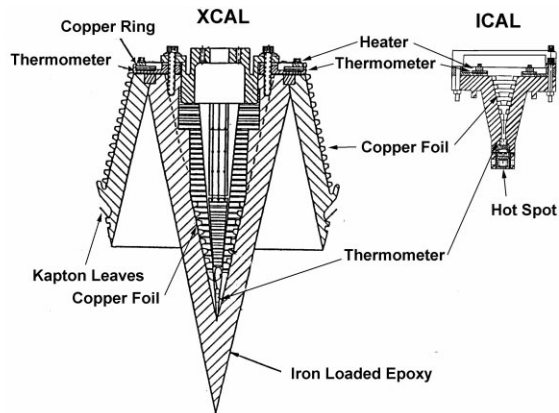


FIG. 2.—Cross section of the FIRAS calibrators. The XCAL is 140 mm in diameter, and the ICAL is 60 mm in diameter. Heaters and thermometers are indicated on the drawing. The Hot Spot heater was designed to null a high-frequency excess in the CMBR. No excess was seen, but the Hot Spot is part of the reason the ICAL has a reflectance of $\sim 4\%$.

sures the difference between the two inputs, this reduced the signal magnitude and relaxed the gain stability and dynamic range requirements of the FIRAS instrument by about a factor of 100.

The true comparison is between the sky and the XCAL, which provides the absolute reference by radiating into the same place with the same temperature (at different times) with all of the other parts of the instrument in similar states. The ICAL has 4% reflections and possible gradients of several mK, but the real requirement on it is that it be repeatable. This was tested over 10 months on sky data as well as calibration data.

There are three requirements for the main calibrator: (1) it must have a well-defined temperature that is known; (2) it must have low reflectivity (emissivity = absorptivity = 1); and (3) it must completely fill the beam (i.e., have no leakage).

2. CALIBRATOR DESIGN AND MATERIAL

The main calibrator is a full-beam temperature-controlled external blackbody that was moved into the aperture on command. It was used for 3 days per month (3 days per week for the last 7 weeks). Its temperature is controlled by a servo loop using an electrical heater and a germanium resistance thermometer (GRT). The control range is 2–25 K, and the temperature was stable to within the GRT resolution of about 0.2 mK $(T/2.7 \text{ K})^3$. The temperature is monitored by three additional GRTs in two separate self-calibrating AC ohmmeter circuits. When not in use, the calibrator is kept in a protected well, with the active surface facing the sky. It is moved by a geared stepper motor.

The calibrator is illustrated in Figure 2. It is 140 mm in diameter, ~ 230 mm long, and shaped like a trumpet mute, with a central peak and a single groove, each with a full angle of $\psi = 25^\circ$. This shape is chosen to suppress specular reflections from the surface. For specular reflections, a ray incident on the calibrator parallel (i.e., visible to the interferometer) to the axis must be reflected from the surface 7 times before it leaves the calibrator region.

The calibrator is machined from two castings of Eccosorb CR-110 (Emerson and Cuming 1980), one for the central peak and one for the remainder, which are glued together

using Eccosorb. This Eccosorb is an epoxy loaded with fine iron powder ($\sim 5 \mu\text{m}$), with an admixture of Cab-o-sil, a fine silica powder ($\sim 10 \mu\text{m}$). The silica powder makes the liquid epoxy thixotropic, so that the iron powder does not settle during the curing process.

The optical properties of the Eccosorb have been reported (Hemmati, Mather, & Eichhorn 1985; Peterson & Richards 1984; Halpern et al. 1986). The normal incidence surface power reflection is approximately $0.08 + (0.06 \text{ cm}^{-1})/\nu$, corresponding to a refractive index of about 2. For the purposes of this paper we will use a refractive index that produces the measured normal incidence reflection. At low temperatures the absorption coefficient was found to be $\alpha \approx 0.3 \text{ cm}^{-1} + 0.45\nu$ over the range of frequencies used here.

At 295 K the absorption coefficient is about twice as large. The manufacturer's literature shows that the permeability approaches unity at high frequencies, and we have assumed it is 1.

To achieve more rapid thermal equilibration, the back surface of the calibrator is covered with 0.25 mm copper sheets. Differential contraction prevents good adhesion, so the copper is perforated to allow the Eccosorb to penetrate it. The copper is corrugated by geared rollers and is cut in the direction perpendicular to the corrugations to make it flexible.

An aluminum foil cap is placed over the back of the copper, since the Eccosorb is not entirely opaque and there are gaps in the coverage of the copper sheets. The back of this structure is covered with a multilayer insulation blanket containing 20 layers of aluminized Kapton separated by layers of Dacron net. This insulation is required because a portion of the calibrator back is exposed to infrared emission from warm portions of the spacecraft, from the Moon, and occasionally from the Earth limb.

The calibrator is designed to have no steady state heat flow through the absorber material, and therefore no temperature gradient. The copper backing is soldered to a copper ring, and the copper ring is attached to the support arm. The temperature of the ring is controlled by the servo, with the electrical heater and the sensor mounted on the ring. This ideal concept is violated in potentially important ways. The copper ring is not mechanically strong, so mounting bolts pass through it into the body of the absorbing material. Also, the manganin thermometer and heater wires are thermal conductors, and they carry some heat away from the calibrator and down the support arm. The heat radiated into the horn by the calibrator is negligible because of the low temperature, and most of it is reflected back to the calibrator. A thermal contact also exists at the calibrator edge. The calibrator does not touch the antenna, leaving a gap of 0.6 mm that is spanned by two ranks of aluminized flexible Kapton leaves 0.1 mm thick and about 12 mm long. The contact force is small, and the estimated thermal contact is small as well. Moreover, under the most important calibration conditions, the antenna was kept at the calibrator temperature, guaranteeing negligible heat flow.

The temperature of various components of the FIRAS is monitored with GRTs. The GRTs are measured with sine wave excitation at two current levels (0.4 and 6.4 μA). The thermometers have separate current excitation and voltage leads, so the lead resistances in the cryostat have little effect on the results. The excitation frequency is 40 Hz, low

enough to minimize shunt capacitance effects. The FIRAS has two separate ohmmeters, each used to read its own set of thermometers. Each ohmmeter circuit includes a stabilized sine wave oscillator and current source, a wideband amplifier, a phase-sensitive detector, and a 14 bit analog-to-digital converter. The input to each ohmmeter is multiplexed through a MOSFET switch, so that it can read 16 thermometers and four calibration resistors, some with both low and high currents, in every major frame of the telemetry (32 s).

The temperature is controlled by a servo loop that uses a separate GRT. The servo provides a choice of thermometer bias currents of 1, 4, 16, and 64 μA to account for the wide range of thermometer resistance over the temperature range 2–20 K ($\sim 7000\text{--}45 \Omega$). It also provides adjustable gain factors of 2^n for $n = 0, \dots, 7$ for both proportional and integral gain. For low temperatures around 2.75 K, the dominant time constant was only 16 s, but at 20 K it was about 14 minutes. The square law nonlinearity of the heater made control of positive temperature steps difficult. The necessary heating power was approximately $(T^2 - T_{\text{min}}^2) \times 100 \mu\text{W K}^{-2}$, where T_{min} was the minimum temperature (about 2.2 K in flight) in the absence of heater power.

3. ERROR ANALYSIS

There are many possible errors at a level of a few parts in 10^5 . The temperature of the Eccosorb must be measured and uniform through the thickness of the material and across the aperture. The reflectance must be small, so that other objects illuminating the calibrator do not contribute significantly to its output. There must be a good seal around the edge, so that radiation from outside does not leak into the beam. Each of these error sources is discussed below.

3.1. Absolute Temperature Scale

The exact temperature of the CMBR is not important for cosmology, since every other cosmological constant is more poorly determined. However, spectrum distortions are important and require the comparison of the results of different instruments. The FIRAS measurement for T_{CMBR} was $2.728 \pm 0.004 \text{ K}$, as described by Fixsen et al. (1996). The uncertainty was entirely due to estimates of systematic errors. In particular, a discrepancy of 4.5 mK between two methods of determining the temperature scale led to the uncertainty estimates. This discrepancy has been resolved allowing a better determination of the CMBR temperature.

The calibrator has three GRTs, two attached to the copper heater ring and one embedded in the Eccosorb tip (see Fig. 2). They disagree by 3 mK, significantly greater than the expected precision of 1 mK. The thermometers were calibrated against a standard thermometer from the National Institute of Standards and Technology, and their calibration was better than 1 mK at that time. Relative to their mean, the three show deviations of -3.3 , -0.3 , and $+3.6 \text{ mK}$ at 2.7 K. Based on only 2 degrees of freedom, this absolute temperature scale has a 1σ uncertainty of 2 mK. At higher temperatures, the GRT at the tip of the cone deviated more from those at the copper ring. The tip GRT was not used in the final calibration.

The ICAL had 2 GRTs in addition to the GRTs used by the temperature control circuitry. Here too the tip GRT read warmer than the GRT at the base. An additional drift of $\sim 3 \text{ mK}$ was noted in the early part of the mission. The

drift was more pronounced in the tip GRT than the base GRT.

To further investigate possible drift in the GRT calibration, a group of 10 thermometers was recalibrated 1.7 yr after the launch, and while seven remained within 1 mK of their original response, three deviated by as much as 6 mK. Some of the recalibrated thermometers were more susceptible to self-heating by the excitation current, a temperature shift proportional to the square of the excitation current. The hermetically sealed helium filling, which helps establish thermal contact, might have leaked out.

The calibrations were made with a 1 Hz square wave excitation, while the flight ohmmeter used 40 Hz sine waves. Direct comparison of the two systems showed an offset of about 7 mK. The explanation of this was not determined. In the comparison experiment neither system was in its final configuration, and either (or both) of them could have been affected by the requirement of long cables to the Dewar, which were not used in flight. Nonlinearities of the flight ohmmeter were measured with the calibration resistors in flight and would not cause an error larger than 0.3 mK at 2.7 K.

The flight ohmmeters used two different excitation currents. These typically had differences of 5 mK, with the higher excitation current reading a higher temperature both in ground tests before the flight and in the flight. The higher excitation current was used at 2.7 K because the lower excitation current had more noise. Averaging over 100,000 samples allows comparison at the 10 μ K level. The offset is not uniform and varies between 2.5 and 7.5 mK on the XCAL thermometers.

The self-heating power at 2.7 K is 110 nW for the high current and 0.4 nW for the low current setting. A temperature change of 5 mK implies a thermal conductivity of 22 μ W⁻¹ K. At higher temperatures the heating is smaller and the thermal conductivity is larger, and thus one is led to expect the self-heating to be only 10% as large at 5 K. This general trend can be seen in the data, but the details are obscured by noise (although there are \sim 100,000 observations at 2.7 K, there are only a few thousand between 2.8 and 5.5 K). Although it is possible to determine the difference between the low and high current readings to 10 μ K, the ultimate accuracy is no better than 1 mK. This correction of 5 mK leads to a new CMBR temperature estimate of 2.725 K rather than the 2.730 K previously reported for the thermometers.

A 5 mK error in the temperature determination of the XCAL leads directly to a 5 mK error in the temperature determination of the CMBR. However, the calibration process corrects other effects of the error to first order (Fixsen et al. 1994).

The FIRAS also allows other determinations of absolute temperatures, based on the wavelength scale and the known shape of the Planck function. The detector noise contribution to the uncertainty of this scale is quite negligible, and the largest known uncertainty is the determination of the wavelength scale. It is derived from FIRAS observations of the interstellar CO and [C I] lines at 1300, 867, 650, and 609 μ m (Fixsen et al. 1996). The temperature scale was determined independently from seven different combinations of the four detectors and four scan modes. These determinations agreed within their uncertainties, and the weighted uncertainty is 0.2 mK. There is an additional common uncertainty of 0.82 mK due to the uncertainty of the fre-

quency scale. The result is 2.7255 K \pm 0.85 mK. With the correction for self-heating, the discrepancy with the GRT measurement is only 0.5 mK, within the uncertainty estimates of either method.

There is yet another determination of the temperature that is independent of the previous two. The FIRAS measured the dipole amplitude, 3.372 \pm 0.007 mK (Fixsen et al. 1996), and the shape of this spectrum was fitted to a $\partial B/\partial T$ with an adjustable temperature, with the result of 2.717 K. The differential microwave radiometer (DMR) on board COBE also measured the dipole amplitude, 3.353 \pm 0.024 mK (Bennett et al. 1996), and the DMR was calibrated independently to 0.5% (Bennett et al. 1992). The DMR calibration was also checked by measuring the dipole effect of the Earth's motion around the Sun. By assuming that the DMR dipole amplitude is correct and that the discrepancy is due to a calibration error, we can correct the FIRAS by dividing the frequency scale by 1.002, which multiplies the dipole temperature by the same factor. The final result is 2.722 K \pm 12 mK, which is 3 \pm 12 mK below the final temperature scale. The uncertainty is dominated by the uncertainty in the DMR calibration.

Averaging these three determinations of the CMBR temperature, $\langle 2725 \pm 1, 2725.5 \pm 0.85, 2722 \pm 12 \rangle = 2725.28 \pm 0.66$ mK. The χ^2 is 0.29 for 2 degrees of freedom. There is reason to be cautious, but a CMBR temperature of 2.725 \pm 0.002 K (95% confidence) is a good description of the CMBR.

3.2. Thermal Gradients

The main thermal requirement for the FIRAS calibrator is uniformity. By design, the calibrator has no steady state heat flows through the absorbing material, so that theoretically there can be no gradients in temperature. The absorber is supported from a copper ring (140 mm diameter, 13 mm wide, and 3 mm thick) whose temperature is regulated by a heater, and heat from the copper ring flows out directly to the helium tank through a strap. However, compromises were required to make the calibrator survive launch vibrations, and the lead wires to the thermometers carry a small amount of heat away from the calibrator. To investigate the effects of these compromises, an accurate copy of the flight calibrator (the flight spare) was built and instrumented with thermometers and heaters. In addition, a finite-element numerical model was devised and adjusted to match the laboratory test data. We report first on the test data, then on the numerical model, and finally give the estimated uncertainties induced by the gradients.

3.2.1. Thermal Gradient Test

The calibrator copy was instrumented with four additional thermometers, as illustrated in Figure 3, and mounted in a helium cryostat suspended by threads in a vacuum. A copper heat strap with a conductance similar to that of the flight calibrator mounting arm and cooling strap connected the calibrator mounting ring to the helium bath. An aluminum shield prevented radiation from warm parts of the cryostat from reaching the calibrator. The thermometers were from the same group as the flight thermometers and were recalibrated before installation (see § 3.1).

Temperature gradients were measured for a range of helium-bath and calibrator temperatures. Residual thermometer calibration problems were still present at the level of \sim 1 mK. They were recognized by turning off the cali-

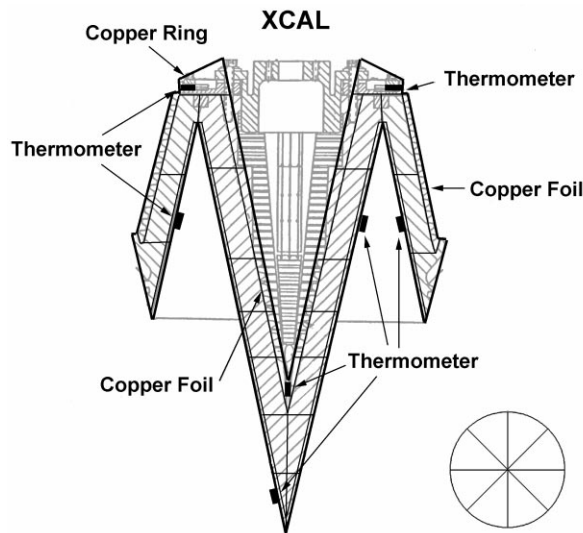


FIG. 3.—Finite-element model of calibrator. There are generally three layers: the copper backing, the iron-loaded epoxy, and the front surface. Each section is repeated for eight elements around the circumference, as shown in the lower right. The additional thermometers on the ground test of the duplicate calibrator are indicated. There were other thermometers on the support arm and the helium bath (not shown). The multilayer insulation on the back (upper surface) is also not shown.

brator heater, so that there should be no genuine temperature gradients, and adjusting the helium-bath temperature to 2.634 K by regulating the helium pressure. The measured calibrator temperature was 2.694 K, confirming that the residual heating sources, such as radiation from the warm sections of the cryostat, were negligible. Then the helium temperature was lowered to 1.5 K while the temperature control servo was activated to fix the calibrator temperature at 2.7 K. The change in measured calibrator temperatures that occurred as the helium bath was cooled are considered to indicate real thermal gradients. Those thermometers mounted together on the copper ring with the heater and control thermometers showed temperature changes of less than 1.3 mK. Those mounted near the tip of the calibrator deep inside changed less than 0.1 mK. Some thermometers were also glued to the surface of the cone that faces the spectrometer. These changed less than 1 mK.

3.2.2. Thermal Gradient Model

These measurements confirm that the temperature gradients within the calibrator material are small but detectable under some circumstances. To understand their origin and to estimate their values in the flight calibrator, we made a finite-element numerical model of the temperatures, as illustrated in Figure 3. Eccosorb has a thermal conductivity of $0.8 \text{ mW cm}^{-1} \text{ K}^{-1}$ (Halpern 1986), while the copper has a conductivity of $2 \text{ W cm}^{-1} \text{ K}^{-1}$ at 3 K. The corrugated copper backing material is 0.25 mm thick, but its lateral conductivity still exceeds that of the thick Eccosorb by a factor of 3. The boundary impedance between the copper and the Eccosorb is not known, and it may be relatively high if the adhesion between them is broken by the differential thermal contraction. The heat capacity of the Eccosorb is $C_p = 0.6T^{2.05} \text{ mJ g}^{-1} \text{ K}^{-1}$ (Peterson & Richards 1984, citing a private communication from M. Halpern), and its mass $\sim 1.5 \text{ kg}$. The slowest time constant is for the ther-

mometer attached to the exterior of the Eccosorb, 16 s at 2.7 K. This implies that the copper-to-Eccosorb conductance is greater than 0.35 W K^{-1} , and the contact area is $\sim 100 \text{ cm}^2$.

There is one significant discrepancy between the model and the actual calibrator. The time constant for the thermometers on the heater ring to sense the change in applied heat is 21 s, which is much longer than the expected value. This causes considerable difficulty in tuning the control servo, since the time delay causes phase shifts that limit the servo gain and hence its speed of response. The time constant could be important to the thermometer accuracy if it indicates that the thermometer is not well attached. In that case, its lead wires would conduct heat from the thermometer down to the helium bath, and the thermometer would read too low. This effect was checked in the calibrator copy and would have been detected unless all the thermometers showed exactly the same amount of error, an unlikely coincidence. It is more likely that the heater itself is not well attached to the ring, which could happen if its adhesive failed at low temperatures. To guard against this failure, a spring plate was added to press the heater against the copper ring in both the flight and copy calibrators. The heater, a Minco resistive film embedded in a Kapton insulating sandwich, provides evenly distributed heat around the copper ring. The adhesion could not be verified in the cooled calibrator because the adhesive becomes sticky again at room temperature.

3.2.3. Thermal Gradient Error

The FIRAS beam may see different parts of the calibrator and penetrate to different depths at different wavelengths. We consider three possibilities, and based on the tests and numerical model, we conclude that these effects are small. To illustrate, we consider sample calculations.

First, consider a radial gradient in calibrator temperature. Our measurements limit such a gradient to $\sim 1 \text{ mK}$. To obtain a first-order spectrum error, we require an antenna pattern that is dependent on both radius and frequency. In geometrical optics there is no reason for such a dependence, and, indeed, the concentrator antenna is a good scrambler. A plausible guess would be that wave effects could cause the low-frequency beam to avoid the walls of the concentrator. Without a detailed calculation, we can still assume a Taylor series expansion in wavelength, but we do not know whether the leading term is linear or higher order. Taking the maximum error as 1 mK at the cutoff wavelength of the antenna $\lambda_0^2 = A\Omega$, we plot the resulting photometric error in Figure 4 for an assumed linear leading term.

Second, suppose that there is a cold spot in the calibrator that is seen through the thickness (12 mm) of the Eccosorb. Such an error could occur if the mounting bolts induce a gradient. Figure 4 shows the error resulting from a spot of area 0.5 cm^2 at a temperature 100 mK different from the average. The attenuation coefficient of the Eccosorb is strongly frequency dependent, so that the resulting error falls rapidly with frequency.

Third, suppose that there is a temperature gradient with depth into the calibrator material. We have no reason to expect this to be a dominant term, since there is no radiative or other heat transport across the surface. Nevertheless, we can evaluate the effect as a function of frequency. The effective temperature is measured at an optical depth of unity into the Eccosorb, i.e., a physical depth of $1/\alpha$. Assuming

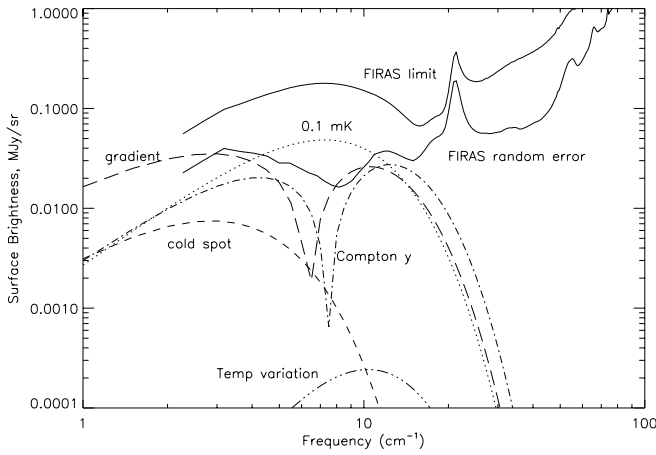


FIG. 4.—Gradient errors for calibrator. The possible errors due to a thermal gradient from the surface to the inside (gradient), a spot 100 mK colder on the back of the Eccosorb, the limits from the measurements of y , and the measured temperature variation are shown. A 0.1 mK temperature change and the FIRAS uncertainties are shown for comparison. The curves with the dip at $\sim 8 \text{ cm}^{-1}$ change sign there and are negative at lower frequency. The 2.7 K blackbody peaks at 400 MJy sr^{-1} .

that the gradient is 1 mK cm^{-1} , we obtain the error plotted in Figure 4.

There is a negligible second-order effect due to possible gradients. The Planck function for the mean temperature is not the same as the mean of the Planck functions for the various parts, because it is not linear in temperature. This effect can be modeled precisely. The Planck function $B_\nu(T)$ can be expanded in a Taylor series around the mean temperature, giving an effective radiated power

$$P_\nu = B_\nu(T) + \Delta T \frac{\partial B_\nu}{\partial T} + \frac{1}{2} \Delta T^2 \frac{\partial^2 B_\nu}{\partial T^2}, \quad (1)$$

where T is the original temperature, ΔT is the mean shift in temperature, and ΔT^2 is the variance of the temperature distribution. We define $x = h\nu c/k_B T$, where h is Planck's constant, ν is the frequency $1/\lambda$, and k_B is Boltzmann's constant. The first and second derivatives are

$$\frac{\partial B_\nu}{\partial T} = B_\nu \frac{x}{T} \frac{e^x}{e^x - 1}, \quad (2)$$

$$\frac{\partial^2 B_\nu}{\partial T^2} = \frac{1}{T} \frac{\partial B_\nu}{\partial T} \left(x \frac{1 + e^{-x}}{1 - e^{-x}} - 2 \right). \quad (3)$$

This is closely related to the cosmological Compton distortion given by Zeldovich & Sunyaev (1969), scaled by the parameter y . A linearized form for the distortion of the spectrum S_ν is

$$\frac{\partial S_\nu}{\partial y} = T^2 \frac{\partial^2 B_\nu}{\partial T^2} - 2T \frac{\partial B_\nu}{\partial T}, \quad (4)$$

$$y = \int \frac{k(T_e - T_\gamma)}{m_e c^2} d\tau_e, \quad (5)$$

where T_e , T_γ and τ_e are the electron temperature, the CMBR photon temperature, and the optical depth to electron Compton scattering. This form preserves the number of photons in the spectrum. Note that any term proportional to $\partial B_\nu/\partial T$ is equivalent to a shift in the mean temperature of the CMBR and still represents a pure blackbody spectrum.

The results found by Fixsen et al. (1996) from the FIRAS data are $y = (-1 \pm 7) \times 10^{-6}$. The corresponding equivalent range of the cosmic temperature distribution is found from $2y = \text{var}(T)/T^2$, where $\text{var}(T)$ is the variance. If we assume that the true CMBR spectrum has $y = 0$, we conclude that the rms variation of the calibrator temperature is therefore less than 15 mK. The limitation from the thermometers is tighter, so any real gradient must be insignificant photometrically.

3.3. Calibrator Reflectance

The calibrator is the dominant radiator in a cavity bounded by four surfaces: the calibrator, the compound concentrator horn, the small aperture of the horn that leads to the spectrometer, and the gap between the calibrator and the concentrator. If all these surfaces were at the temperature of the sky, and the sky were a blackbody, then the radiation inside the cavity would be perfect blackbody radiation and would have the same intensity and spectrum as the sky radiation. In that case, moving the calibrator in or out of the beam would make no change of the radiation field. This is the basis for a precise differential comparison of the sky to the blackbody.

The leading deviations from the perfection of this blackbody cavity are as follows. First, the transmission of the horn for the emission from the calibrator is not unity, but it is absorbed in the gain constants of the spectrometer by the calibration algorithm. Second, the horn is not always at the same temperature as the sky or calibrator, but this is also included in the instrument model, and the horn emission is measured in the calibration process. The calibration process also includes terms for emission from the dihedral, the collimating mirrors, and the bolometer itself. The leading term that is not included in the calibration model is the change in the emission of the instrument, at a temperature of about 1.5 K, that is induced by inserting the external calibrator. This term cannot be included in the calibration model, because the calibrator must be inserted to calibrate and must be out of the horn to view the sky. To first order, the error introduced is

$$dP = [B(T_i) - B(T_c)]r_i, \quad (6)$$

where dP is the error in emitted intensity, B is the Planck function, T_i and T_c are the instrument and calibrator temperatures, and r_i is the reflectivity of the calibrator for radiation originating in the instrument and reflected back toward it.

3.3.1. Reflectance Measurement

Direct measurements of the calibrator reflectance in the same geometrical configuration used in flight were made, but at room temperature. The refractive index of the Eccosorb is nearly the same at room temperature and when cold, so the diffraction and surface reflection should be the same. A coherent microwave system was built to illuminate a duplicate calibrator through a duplicate of the flight antenna. Measurements were made from 30 to 37 GHz and at 93.6 GHz (Fig. 5). Radiation from a source passes through an attenuator and a frequency meter to a "magic tee" microwave beam splitter. From the tee, radiation splits between the two arms of the magic tee. One arm is terminated with a load, and the other has a waveguide leading to the small end of the FIRAS antenna. A rectangular-to-circular transition couples the guide to the antenna at the 0.78 cm

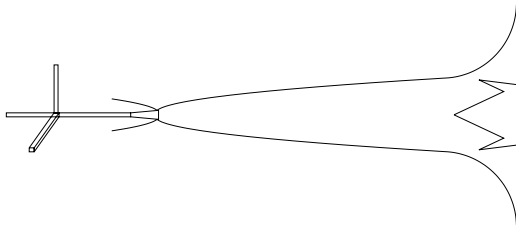


FIG. 5.—Schematic of the setup to measure the reflection of the calibrator. At the left is the magic tee, which has four ports connected to (*left*) a load, (*top*) the detector, (*front*) an oscillator source, and (*right*) a rectangular to cylindrical transition. The circular waveguide has a conical horn to match it to the throat of the horn. The elliptical section of the horn is not used. The calibrator is moved near its nominal position (*at the far right*) to measure the reflection. Measurements were done at 33 and 94 GHz. See text for details.

diameter throat aperture. The radiation is collimated by the antenna and is incident on the calibrator in its usual position. Radiation reflected from the calibrator returns along its path, and some of it is split off by the “magic tee” to the detector. At that point, it interferes coherently with the other signals already present. The total intensity reaching the detector depends on the phase and amplitude of the radiation reflected from the calibrator.

The calibrator was moved along the axis of the antenna to vary the phase of its reflection, which interferes with the larger reflections from the joints and other parts of the setup, producing a sinusoidal interference pattern that clearly identifies the part due to the calibrator reflection. The calibration of the method was made by substituting a flat metal plate for the calibrator. The amplitude was also measured as a function of the angle between the calibrator axis and the antenna axis (Fig. 6). The response was greatest when the angle was zero, and there was no pronounced structure between the measured points. The peak response was -55.8 ± 1.5 dB at 33.4 GHz and -59.0 ± 1.5 dB at 93.6 GHz. The frequency was also swept from 30 to 37 GHz to search for resonant enhancement effects. The response was greater at 35.25 and 36.86 GHz, where it was increased to -45.8 ± 1.5 dB at zero tilt angle.

Note that the test apparatus differs from the flight configuration in an important way: the flight antenna receives $n = 2A\Omega v^2$ modes, but the waveguide system receives only

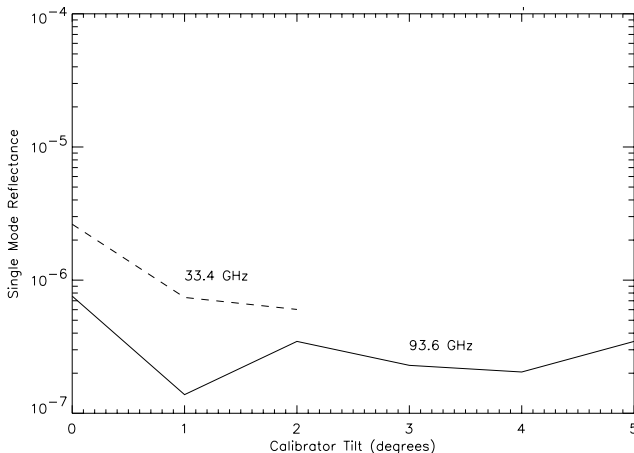


FIG. 6.—Measured calibrator reflectances at room temperature. Plotted here are the measured reflectances as a function of tilt of the calibrator for 33 and 94 GHz. (See also Fig. 5.)

one. For 33.4 and 93.6 GHz, these values are $n = 3.7$ and 29. Also, the multimode concentrator illuminates the calibrator over a range of angles and accepts reflected radiation for the same range. Therefore, the response pattern, which is obtained with a single-mode system and a plane-wave illumination, should be convolved twice with the measured beam profile to obtain a suitable average. The computed effective power reflectance based on these data is 3×10^{-6} at 33.4 GHz and 9×10^{-6} at 93.6 GHz. Unfortunately, the angular response pattern was not measured at 35.35 and 36.86 GHz, so to be conservative we increase the estimated reflection at those frequencies by a factor of 10, giving 3×10^{-5} for the effective reflectance. The interpreted measurements are all less than $3 \times 10^{-5} \text{ cm}^{-1}/v$, which, as we shall see below, is about as expected from diffraction calculations. They are also too small to be detected in the FIRAS photometry.

3.3.2. Diffractive Reflectance

The diffraction of radiation at the calibrator was modeled using the simple Huygens principle for scalar waves (Levy & Keller 1959). We assume that an incident plane wave comes up the concentrator horn, and calculate the field incident on the calibrator surface. The undisturbed plane wave would not diffract back toward the source in a simple cylindrical pipe, so we use the reflected wave amplitude as the effective source for the calculation. To account for polarization effects at the first surface reflection, we use the rms value for the two amplitude reflection coefficients. To account for the multiple reflections of the waves as they go into the groove, we calculate the sum of the amplitudes of all the specularly reflected waves, up to seven reflections. This enhancement is only a factor of 1.1 in amplitude and is applied to the incident amplitude after multiplication by a Gaussian to connect it smoothly with the rest of the surface.

The numerical integration was performed in cylindrical coordinates. The integral with respect to angle yields a Bessel function of zero order. The integral with respect to radius was done numerically with 10,000 steps. The results are plotted in Figure 7. They show a dependence on angle that resembles the Bessel functions, as expected, but do not show the same details as the experimental results. Follow-

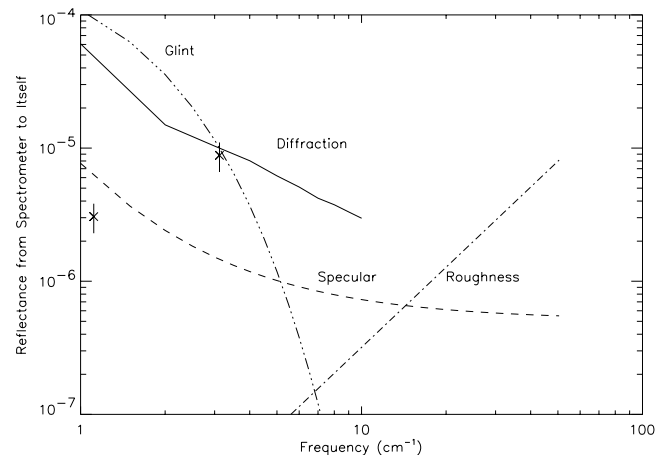


FIG. 7.—Calibrator reflectances for FIRAS. Shown here are plots of the reflectances vs. frequency for several modes of reflection. The crosses with error bars are the measurements at 33 and 94 GHz. Other lines are calculations. See text for details.

ing the same prescription as for the experimental data, we also computed the mean reflection coefficients averaged over the solid angles of the source and the receiver antenna. These are also plotted in Figure 7, and are approximated by $3 \times 10^{-5} \text{ cm}^{-1}/\nu$. There is reasonable agreement between the theory and the measurements, considering the number of approximations made in both.

3.3.3. Specular Surface Reflectance

To estimate the specular reflectance of the calibrator, we approximate it by a V groove of the same included angle in an infinitely thick medium. In this case, there is no mixing of polarizations and all the angles of incidence are known. A ray originating in the spectrometer will be reflected seven times before exiting the V groove, at angles from the normal of $+12^\circ.5$, $-37^\circ.5$, $+62^\circ.5$, $-87^\circ.5$, $+112^\circ.5$, $-137^\circ.5$, and $+162^\circ.5$, where the plus sign indicates reflection away from the center axis and the minus sign indicates reflection toward the center axis. We estimate the refractive index from the normal surface reflectance R_s and use the Fresnel formulae to compute all the reflectances. Averaging over polarizations gives $R_{\text{spec}} = 5 \times 10^{-5}$ at 1 cm^{-1} .

Only a fraction of the returned specular beam is directed back toward the spectrometer. The horn defines a circular field of view of 7° diameter, so one may consider that it sends a circular bundle of rays toward the V groove. The circle comes back shifted by 5° because of the accumulated effect of the 7 reflections, so that it overlaps slightly with the circle representing the rays that can be received by the instrument. The fraction of the area that overlaps is computed as 14%. In other words, if the calibrator were a V groove of two mirrors, 14% of the beam originating in the spectrometer would return to it to be detected. Since the actual calibrator is not a simple V groove, the overlap fraction could be either smaller or larger, but the computation is not precise enough to merit detailed attention. The final effective specular reflection is then 7×10^{-6} , which is comparable to the diffractive term at about 4 cm^{-1} .

3.3.4. Diffuse Surface Reflectance

The surface texture is similar to that of a machined metal surface having a surface roughness of $\sigma = 5 \text{ }\mu\text{m}$ rms. We approximate the calibrator diffuse reflectance by $R_{\text{surf}} = 4R_n(\Omega/\pi) \sin(\psi/2)(\sigma k)^2$, where $k = 2\pi/\lambda$ is the wavevector, $R_n \approx 0.1$ is the normal reflectance of a polished surface, $\psi = 25^\circ$ is the full angle of the cone and groove, and the sine function accounts for the angle of incidence of radiation from the spectrometer. Evaluating at a wavelength of 1 mm , we find $R_{\text{surf}} = 3.2 \times 10^{-7}$, quite negligible, showing that a more exact calculation is unnecessary.

3.3.5. Internal Reflection

The Eccosorb is not thick enough (12 mm) to be entirely opaque, so at centimeter wavelengths the back surface is partly visible through it. The back surface is partly covered with irregularly shaped copper foils. We take its surface reflectance to be unity with a Lambertian angular distribution inside the Eccosorb. $R_{\text{back}} = (\Omega/n^2\pi)T_s^2 \cos \phi e^{-2\alpha t}$, where $T_s = 1 - R_s$ is the transmittance of the front surface, α is the measured absorption coefficient of the material, and t is the thickness. The factor $1/n^2$ accounts for the change in beam divergence at the refractive surface, and the $\cos \phi$ accounts for the spreading out of the radiation over the larger surface inside the material, with $\phi = 77^\circ.5$. The

surface transmittance is evaluated for an angle of incidence of $77^\circ.5$ from the normal. Evaluating this at $\nu = 1 \text{ cm}^{-1}$, we find $R_{\text{back}} = 2 \times 10^{-5}$. This number is already negligible at this frequency because of the relatively lower sensitivity of the FIRAS, and it decreases exponentially as the frequency increases.

The back surface reflections would be much more important if there were a specular glint within the material. The Eccosorb shape is too complex to be amenable to easy calculation. As an example to show the scale of the problem, consider a glint. Because of the symmetry of the calibrator, a ray from the spectrometer can refract and reflect all the way back to the instrument. The net reflectance of such a spot would be governed by a simple formula in the geometrical optics limit: $R_{\text{spot}} = T_s^2 r_{\text{spot}}^2 / r_{\text{cal}}^2 e^{-2\alpha t}$. If we assume that $r_{\text{spot}} = 0.3 \text{ cm}$ is an effective spot radius and that $r_{\text{cal}} = 7 \text{ cm}$ is the calibrator radius, this gives 2.4×10^{-4} at 1 cm^{-1} , which is not as small as other terms calculated above. The estimates from this formula are plotted in Figure 8. At room temperature, the attenuation coefficient of the material is twice as large as at low temperatures, so in the laboratory test such a spot would have given a reflectance of only 3.5×10^{-5} . This is comparable to the directly measured maximum values in the 30–37 GHz band, and therefore it might be a real possibility.

3.4. Horn Emission

Reflection of the horn emission by the calibrator would be significant if the horn temperature were not controlled to match the calibrator temperature. Its emissivity is small, but its area is large. To first order, it causes an error $dP_h = [B(T_h) - B(T_c)]\epsilon_h r_h$, where dP_h is the error in emitted intensity, B is the Planck function, T_h and T_c are the horn and calibrator temperatures, ϵ_h is the horn emissivity toward the calibrator, and r_h is the reflectivity of the calibrator for radiation originating in the horn and reflected toward the instrument. We measured the horn emissivity in the calibration process (Fixsen et al. 1994), and it is small at low frequencies: $\epsilon_h \approx 0.012 + 0.0015(\nu/1 \text{ cm}^{-1})$. We also set T_h to match T_c within 20 mK. The error introduced here can be compared to that from the instrument radiation described

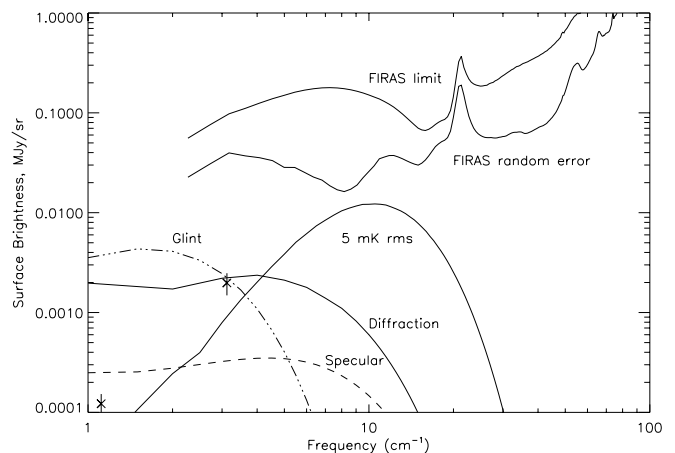


FIG. 8.—Photometric errors for calibrator due to reflectances. The terms fall off at high frequency because all of the emitters in the FIRAS instrument are below 3 K. The crosses with error bars are the measurements at 33 and 94 GHz.

above:

$$\frac{dP_h}{dP} = \frac{B(T_h) - B(T_c)}{B(T_i) - B(T_c)} \frac{\epsilon_h r_h}{r_i} \quad (7)$$

Conservatively assuming that the ratio of reflectances is unity, we still find that the error from horn emission and calibrator reflectance is small relative to the error from instrument emission and calibrator reflectance.

The curious reader might also ask about the emission from the part of the antenna located above the calibrator. This term is negligible for three reasons: the emissivity of the surface is small, the antenna quickly curves away from contact with the main beam, and, finally, the antenna is maintained at the temperature of the sky so that its emissions compensate for the sky radiation that it absorbs. To be quantitative, we use the measured emissivity of the antenna. A simple approximation for the horn emissivity shows that it should be proportional to the surface resistance and the effective length-to-diameter ratio $\int dx/D$, where x is the coordinate along the length and D is the diameter. Without doing a proper calculation of the effects of the curvature, it is reasonable to estimate that the effective length-to-diameter contribution of the horn flare is less than 1% of the total, so that its emissivity should be less than a few parts in 10^4 . As stated above, its temperature is also well known and kept within 10 mK of the sky temperature, and therefore this error is less than a few parts in 10^6 .

3.5. Edge Leakage

To prevent wedging the calibrator into the horn in flight, we required a clearance between them. The gap, about 0.06 cm, could cause errors in the calibration. In addition, there is a similar area of the Eccosorb rim that could not be covered completely with aluminum foil and multilayer insulation, and some radiation could be transmitted through it. The sources of warm radiation in flight are the multilayer insulation blanket on the outside of the calibrator and its support arm, the radiation emitted by the sunshade and scattered downward by the arm, and the far-infrared sky, including the Moon, which shone onto the top of the calibrator for half of each calibration orbit.

3.5.1. Leakage Measurement

We begin with the measurements and then make theoretical extrapolations and interpretations. There were three kinds of measurements, some taken on the ground with a warm cryostat dome above the instrument, the ordinary calibration data in flight, and finally some data taken in flight with the calibrator moved progressively farther out of the antenna.

The ground data were taken with the FIRAS in the flight cryostat and oriented so that the calibrator could be moved in and out step by step. First, the FIRAS observed the warm dome of the cryostat at a temperature near 40 K. The instrument calibration showed that the warm dome had an effective emissivity of $\sim 10\%$. Second, the calibrator was put in place, the servo was controlled to a fixed temperature around 13 K, and 1 hr of observations were taken. Then the calibrator was moved out in steps, with 1 hr of data at each position. A single step corresponds to about 1.4 mm of motion. Data were taken for positions 1, 3, 6, and 8 steps from the origin. The broadband leakage in the low-frequency channel ($1\text{--}20\text{ cm}^{-1}$) was measured by the height

of the peak of the interferogram. Relative to the signal level seen observing the dome directly, the peak height was approximately $(1.2n^2 \pm 2) \times 10^{-6}$, where n is the number of steps taken from the nominal position. Similar analysis of the high-frequency channel ($20\text{--}100\text{ cm}^{-1}$) yielded a factor of $(3n^2 \pm 35) \times 10^{-6}$. Other observations were done with the calibrator at 4 K and while varying the dome temperature from 5 to 66 K. These showed no evidence of leakage around the calibrator.

We conclude that the attenuation is good when the calibrator is all the way into the horn and that it gets rapidly worse when it is pulled out far enough for the flexible leaves to lose contact. The evidence for the quadratic dependence on n is weak, given the signal-to-noise ratio. For further calculation we assume that when the calibrator is in place, the correct number is 4×10^{-6} in both low- and high-frequency bands. This is a reasonable number, corresponding to an illuminated gap area that is 2% of the total calibrator area and an attenuation factor of about 1.4% for each row of flexible leaves.

A test was also done in flight by removing the calibrator 12 steps, or 17 mm, from the horn. Only a few interferograms were taken, but there was no sign of a change of signal level. Calculations based on the ground test data (see below) showed that it should be impossible to observe any signal without spending a large fraction of the mission on this test and that, in any case, this test would not be relevant to the situation where the calibrator is in its proper position. This test produces a weak limit, illustrated in Figure 9. The limits found from the flight test were extrapolated from $n = 12$ to $n = 1$ according to the n^2 form found in the ground tests, and they are plotted as a horizontal line since no spectral information was obtained. While suggestive, this cannot be considered a firm limit.

The flight calibration data are sensitive to leakage at high frequencies, because most of the calibration data were taken with both calibrators and both antennas controlled to 2.7 K. With temperatures this low, there is nothing in the instrument that can emit significantly above 30 cm^{-1} , so any signal seen there must be an instrument error. We used all the data taken in this configuration and computed the residuals from the calibration model. The spectrum of the residuals is nearly flat and the noise is limited except near 73 cm^{-1} , where there are residual effects of the coherent instru-

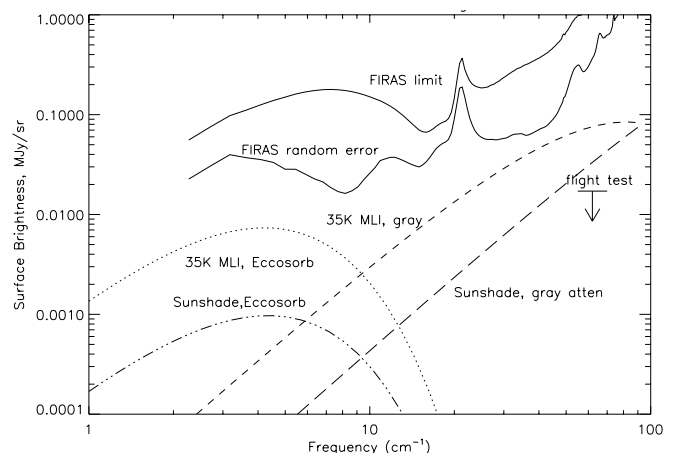


FIG. 9.—Calibrator error due to leakage. The sunshade is assumed to heat the insulation layer to $\sim 35\text{ K}$.

ment vibrations. The weighted rms residual was $0.008 \text{ MJy sr}^{-1}$ from 55 to 70 cm^{-1} . A limit can also be obtained by fitting an assumed spectrum to the residual.

3.5.2. Leakage Interpretation

To use these broadband limits and measurements, we must assume the effective spectral shape of the radiation leakage. The incident radiation comes from the multilayer insulation above the calibrator, from the sunshield and the calibrator support arm, from the Moon, and from the general far-infrared sky. The spectra for the warm cryostat dome (measured on the ground) and for the Moon are reasonably accurate, but the multilayer insulation emission and scattered sunshield emission are order-of-magnitude estimates.

The blanket temperatures are quite uncertain but important. They are unmeasurable, because the blankets are so thin and light that a thermometer attachment would completely change their thermal properties. The insulation near the calibrator is exposed only to radiation from the sky and should always be quite cold, but the insulation on the sides of the support arm sees radiation from the interior of the sunshield at 180 K . An unsupported graybody at this location would reach a temperature of about 40 K , based on the view factor and the emissivity of the sunshield, which is assumed to be 0.05 . The thermal conductance between the blanket layers and laterally to the corners where they are attached is sufficient to lower the temperatures to about 4 K , but this calculation is also quite uncertain and cannot be proved. To be conservative, we assume that the blanket temperature is 35 K . The emission of the blanket toward the calibrator is assumed to have an emissivity of $0.003 \nu^{0.5}$ (approximately twice the calculated value for good aluminum at room temperature) and to fill 10% of the solid angle at the top of the leaking area. Using these assumptions, the ground test data can be extrapolated to the flight case and are plotted in Figure 9. Another curve, labeled $35 \text{ K MLI Eccosorb}$, shows the effect of the same assumed incident radiation field, transmitted into the Eccosorb at its exposed rim and attenuated as it goes through. This response turns

sharply down at high frequency because of the increasing Eccosorb absorption coefficient.

The calibrator support arm can scatter radiation downward. To estimate this we assume that the sunshade has the same emissivity as the insulation blankets, with two stages of geometric attenuation. First, the sunshade subtends only about 0.15 sr as seen from the calibrator arm. Second, the radiation scattered by the arm edge is attenuated by a factor of 0.05 to allow for the divergence of the scattered ray bundle from the arm. The net brightness is an order of magnitude less than the emission from the multilayer insulation if it is at 35 K . These assumptions produce a pair of curves similar to those for the multilayer insulation.

If any of the leakage sources were important in flight, our calibration with cold calibrator sources would have revealed an offset at high frequencies. No such offset was observed. The limit for this measurement is shown in Figure 9.

4. SUMMARY AND CONCLUSIONS

The calibration methods for the Far Infrared Absolute Spectrophotometer (FIRAS) have been described and the accuracy estimated. The improvement in the estimation of the uncertainty allows an improved absolute temperature measurement of $2.725 \pm 0.002 \text{ K}$ (95% confidence). This estimate does not disagree with earlier measurements, which are less precise. The calibrator errors are all estimated to be smaller than the measured CMBR spectrum distortion limits reported by Mather et al. (1994), Fixsen et al. (1996), and Fixsen et al. (1998).

We thank A. Murdoch and H. Hemmati for their detailed measurements of the optical properties of Eccosorb and for the reflectivities and transmissions of the calibrator assemblies through several generations of designs. W. Eichhorn made ray traces of the horn. The calibrator was machined in the GSFC shops, and C. Clatterbuck developed the recipes for mixing and casting the Eccosorb blocks.

REFERENCES

- Bennett, C. L., et al. 1992, *ApJ*, 391, 466
 ———. 1994, *ApJ*, 436, 423
 ———. 1996, *ApJ*, 464, L1
 Boggess, N. W., et al. 1992, *ApJ*, 397, 420
 Brodd, S., Fixsen, D. J., Jensen, K. A., Mather, J. C., & Shafer, R. A., eds. 1997, *COBE Ref. Pub. 97-C, COBE Far Infrared Absolute Spectrophotometer (FIRAS) Explanatory Supplement* (Greenbelt, MD: NASA/GSFC); available in electronic form from the NSSDC
 Emerson and Cuming (Canton, MA). 1980, *Tech. Bull. 2-6* (revised)
 Fixsen, D. J., et al. 1994, *ApJ*, 420, 457
 ———. 1996, *ApJ*, 473, 576
 ———. 1997, *ApJ*, 486, 623
 ———. 1998, *ApJ*, 508, 123
 Halpern, M., et al. 1986, *Appl. Optics*, 25, (4) 565
 Hemmati, H., Mather, J. C., & Eichhorn, W. L. 1985 *Appl. Opt.*, 24, 4489
 Levy, B. R., & Keller, J. B. 1959, *Comm. Pure Appl. Math. Commun.*, 12, 159
 Mather, J. C. 1981, *IEEE Trans. Antennas and Propagation*, AP-29, 967
 ———. 1982, *Opt. Eng.*, 21, 769
 ———. 1987, *Proc. 13th Texas Symp. on Relativistic Astrophysics*, ed. Ed Ulmer (Chicago: World Scientific), 232
 Mather, J. C., Fixsen, D. J., & Shafer, R. A. 1993, *Proc. SPIE*, 2019, 168
 Mather, J. C., Toral, M., Hemmati, H. 1986 *Appl. Opt.*, 25, 2826
 Mather, J. C., et al. 1994, *ApJ*, 420, 440
 Martin, D. H., & Puppelt, E. 1970, *Infrared Phys.*, 10, 105
 Miller, M. S., Eichhorn, W. L., & Mather, J. C. 1982, *Opt. Lett.*, 7, 210
 Mosier, C. L. 1991, (AIA 91-0362) (Greenbelt: NASA)
 Peterson, J. B., & Richards, P. L. 1984, *Int. J. Infrared Millimeter Waves*, 5, 1507
 Welford, W. T., & Winston, R. 1978, *The Optics of Nonimaging Concentrators* (New York: Academic)
 Wright, E. L., et al. 1994, *ApJ*, 420, 450
 Zeldovich, Ya. B., & Sunyaev, R. A. 1969, *Ap&SS*, 4, 301